Electronic Supplementary Material (ESI) for Physical Chemistry Chemical Physics.

Supporting Information

Predictive Morphology, Stoichiometry and Structure of Surface Species in Supported Ru Nanoparticles under H_2 and CO atmospheres from Combined Experimental and DFT Studies

Aleix Comas-Vives,[a*] Karol Furman,[a] David Gajan,[b] M. Cem Akatay,[c] Anne Lesage,[b]
Lyndon Emsley,[b,d] Fabio H. Ribeiro,[c] Christophe Copéret.[a*]

[a] ETH Zürich, Department of Chemistry and Applied Biosciences, Vladimir-Prelog-Weg 1-5, CH-8093 Zürich, Switzerland.

[b] Centre de RMN à Très Hauts Champs Institut des Sciences Analytiques Université de Lyon (CNRS/ENS Lyon/UCB Lyon 1) 5, rue de la Doua, 69100 Villeurbanne, France

[c] Purdue University, School of Chemical Engineering, Forney Hall of Chemical Engineering, 480 Stadium Mall Drive, West Lafayette, IN 47907-2100, USA.

[d] EPFL SB ISIC LRM, BCH 1530 (Batochime UNIL), Av. F.-A. Forel 2, CH-1015 Lausanne, Switzerland.

1. Experimental and Computational details

1.1 Catalyst preparation. Ru nanoparticles (Ru NPs) supported on SiO_2 (S_{BET} = 200 m^2/g), SBA-15 (S_{BET} = 800 m^2/g) and SiO_2-spheres (S_{BET} = 35 m^2/g) were prepared via incipient wetness impregnation (IWI) of an aqueous solution of $[Ru(NO)(NO_3)_3]$ on aforementioned supports. Prior to impregnation, all supports were calcined at 500 °C in ambient air and then dehydroxylated at 500 °C under vacuum (10^{-5} mbar) for 12h. Impregnated samples were dried in a flow of synthetic air at 120 °C (1 °C/min) for 6h and reduced at 400 °C (0.5 °C/min) for 6h with pure H_2 (38 mL/min). After reduction, H_2 was evacuated at room temperature (10^{-5} mbar) for 1h, and samples were stored in dry and oxygen-free glove-box. Since the surface area (S_{BET}) of supports varied from one to another, in order to obtain a comparable density of RuNPs homogenously dispersed on all supports, three different loadings of Ru were targeted: 3 % wt., 15 % wt. and 0.3 % wt. for Ru/SiO_2, Ru/SBA-15 and Ru/SiO_2-spheres, respectively.

1.2 N_2 – adsorption at -196 °C. N_2 – adsorption isotherms were measured at -196 °C using BelMini apparatus. Samples were loaded inside the glove-box and connected to BelMini apparatus without exposure to air. Brunauer-Emmett-Teller (BET) method was used to calculate the surface area of studied samples.

1.3 High-angle annular dark-field scanning transmission electron microscopy (HAADF-STEM) and high-resolution transmission electron microscopy (HR-TEM) study. The electron microscopy study was performed on a HD2700CS microscope (Hitachi, aberration-corrected) with 200 kV acceleration voltage in the HAADF-STEM mode resulting in atomic number contrast (Z contrast). After an exposure to ambient air the sample were place on a lacey carbon grid. The particle size distribution was estimated by statistical analysis on *ca.* 200 particles. Ruthenium dispersion, defined as the molar ratio between surface metal and bulk metal, was calculated back from HAADF-STEM particle size distribution. A full oxidation of ruthenium to RuO_2 after exposure to air was assumed.[1] High-resolution transmission electron microscopy study (HR-TEM) was performed on 80-300 kV S/TEM FEI Titan microscope operating at 300 kV.

1.4 H_2 and CO chemisorption measurements. Chemisorption experiments were carried out on a Belsorb-Max device from BEL Japan. In a measuring cell, around 150 mg of catalyst were pretreated at 10^{-6} mbar at 350 °C for 3 h using a ramp of 1 °C/min. All chemisorption measurements were performed at 25 °C after the pretreatment. In all cases, the pressures at equilibrium were recorded when the pressure variation was below 0.03% per minute. The particle size estimations were based on a *hcp* geometry, assuming complete reduction of the metal.[1,2] The quantification of surface ruthenium was calculated from the adsorption at saturation deriving from a dual Langmuir adsorption model.[3] H_2 and CO chemisorption on metal-free silica supports were performed and adsorbed negligible amounts of gas.

1.5 CO adsorption on Ru/SiO_2 studied by FTIR spectroscopy. Prior to adsorption of CO, Ru/SiO_2 was thermally treated at 350 °C for 6 h (1 °C/min) under high vacuum (10^{-5}

mbar). Subsequently, an excess of carbon monoxide was introduced at 25 °C to the sample cell containing Ru/SiO_2. After 5 h, the gas phase was evacuated for 1 h at 10^{-5} mbar, and the sample was placed into the glove-box, pressed into a thin pellet using a 7-mm die set. The IR spectra were recorded on a Bruker Alpha-T spectrometer in a transmission mode with 24 scans at a resolution of 4 cm^{-1}.

1.6 ^{13}CO adsorption on Ru/SBA-15 studied by solid-state ^{13}C nuclear magnetic resonance (solid-state ^{13}C NMR). Prior to adsorption of ^{13}CO, Ru/SBA-15 was thermally treated at 350 °C for 6 h (1 °C/min) under high vacuum (10^{-5} mbar). Subsequently, an excess of ^{13}CO was introduced at 25 °C to the sample cell containing Ru/SBA-15. After 5 h, the gas phase was evacuated for 1 h at 10^{-5} mbar, and the sample was placed into the glove-box where it was packed into the NMR rotor. All solid-state ^{13}C NMR spectra were recorded on a Bruker AVANCE III 700 MHz spectrometer using a 2.5 mm MAS HX probe. Chemical shifts are reported in ppm downfield from liquid $SiMe_4$ (0 ppm).

1.7 Computational details. Plane-wave, gradient-corrected periodic DFT calculations were carried out using the Vienna Ab initio Software Package (VASP).[4] The constructed nanoparticles were optimized using the VASP code by means of the PBE exchange correlation functional.[5] The periodic augmented wave (PAW) method[6] was adopted for describing the electron-ion interactions with an energy cutoff equal to 400 eV. The cohesive energy per Ru atom was computed for every nanoparticle shape referenced to the energy a single Ru atom in VASP. The CP2K was used in order to evaluate the CO and H_2 chemisorption in combination with the revised version of the PBE density functional[7] for CO chemisorption and the PBE functional for H chemisorption. The DZVP was used for Ru atoms and the TZV2P basis sets for C, O and H atoms. For the calculations of the Ru001 surface, a 4x4 unit cell with three metallic layers was used fixing the bottom layer. The binding energy E_{bind} per n CO molecules or n H atoms were calculated using the following expressions:

$$E_{\mathrm{bind}}/_{\mathrm{CO}} = (E_{\mathrm{NP\text{-}nCO}} - E_{\mathrm{NP}} - \mathrm{n}_{\mathrm{CO}} E_{\mathrm{CO}})/n_{\mathrm{CO}},$$

where $E_{NP\text{-}CO,}$ E_{NP}, E_{CO} are the energies of the nanoparticle-adsorbate, nanoparticle and a CO molecule, respectively. For the case of H, the energy of adsorption per H was referenced to the energy of 1/2 H_2 molecule, as shown in the following expression.

$$E_{\text{bind}}/\text{H} = (E_{NP\text{-}nH} - E_{NP} - (n_H/2)E_{H2})/n_H$$

in which $E_{NP\text{-}H,}$ E_{NP}, E_{H2} are the energies of the nanoparticle-adsorbate, the nanoparticle and a H_2 molecule, respectively. The ΔG energies for CO and H chemisorption processes were obtained using the *ab initio* atomistic thermodynamics approach as described by Reuter and Scheffler[8] with the use of thermochemical tables.[9] Zero point energy corrections were included for the case of H.

$$\Delta G = E_{NP\text{-}nCO} - E_{NP} - n_{CO}\mu_{CO}$$

where $\mu_{CO} = E_{CO} + \Delta\mu_{CO}$

$$\Delta G = E_{NP\text{-}nH} - E_{NP} - n_H\mu_H$$

$$\mu_H = 1/2E_{H2} + \Delta\mu_H$$

The chemical potential of CO and H are directly related to the temperature (T) and the CO and H_2 pressures; P_{CO} and P_{H2}. Finally, the frequency analysis was performed as implemented in the CP2K code, considering the only the displacement of the CO molecules adsorbed on the Ru nanoparticle.

2. Additional Data

S1. H_2 chemisorption on supported RuNPs (raw data).

Table S1a. Raw data for H_2 chemisorption on $RuSiO_2$.

No.	Pe/kPa	P0/kPa	Vd/mL	V/mL(STP) g-1
1	1.33E-02	101.3	18.135	1.45
2	5.63E-01	101.3	18.135	1.92
3	2.2977	101.3	18.135	2.10
4	4.5205	101.3	18.135	2.19
5	7.8073	101.3	18.135	2.28
6	11.132	101.3	18.135	2.34
7	18.906	101.3	18.135	2.45
8	29.825	101.3	18.135	2.5128

Table S1b. Raw data for H_2 chemisorption on Ru/SBA-15.

No.	Pe/kPa	P0/kPa	Vd/mL	V/mL(STP) g-1
1	4.56E-03	101.3	11.936	2.77E+00
2	7.67E-03	101.3	11.936	5.41E+00
3	3.63E-01	101.3	11.936	7.28E+00
4	5.56E-01	101.3	11.936	7.51E+00
5	2.3815	101.3	11.936	8.38E+00
6	4.7234	101.3	11.936	8.86E+00
7	8.3484	101.3	11.936	9.28E+00
8	11.357	101.3	11.936	9.5476
9	20.01	101.3	11.936	10.059
10	31.181	101.3	11.936	10.551

Table S1c. Raw data for H_2 chemisorption on Ru/SiO_2-spheres

No.	Pe/kPa	P0/kPa	Vd/mL	V/mL(STP) g-1
1	5.34E-01	101.3	11.027	1.54E-01
2	2.76E+00	101.3	11.027	1.80E-01
3	4.7961	101.3	11.027	1.77E-01
4	8.4211	101.3	11.027	1.92E-01
5	11.664	101.3	11.027	1.98E-01
6	20.329	101.3	11.027	2.15E-01
7	31.551	101.3	11.027	2.27E-01

S2. Parameters of the Langmuir fit for supported RuNPs (H_2 chemisorption).

The H_2 chemisorption data was fitted with dual dissociative Langmuir model (eq. 1):

$$Q_{max} = Q_{ads,1}\frac{\sqrt{K_1P}}{1+\sqrt{K_1P}} + Q_{ads,2}\frac{\sqrt{K_2P}}{1+\sqrt{K_2P}} \quad \text{(eq. 1)}$$

where Q_{max} corresponds to the amount of H_2 adsorbed at saturation, Q_{ads} stands for the quantity of H_2 adsorbed at pressure P, and K represents the equilibrium constant.

Table S2. Parameters of the dual dissociative Langmuir for supported RuNPs (H_2 – chemisorption).

Sample	$Q_{ads,1}$ **[mole$_{H2}$/g$_{cat}$]**	**K_1**	$Q_{ads,2}$ **[mole$_{H2}$/g$_{cat}$]**	**K_2**	Q_{max} **[mole$_{H2}$/mole$_{Ru}$]**	R^2
Ru/SiO_2[a]	0.100	0.006	0.08	686.1	0.62	0.99
Ru/SBA-15[b]	0.623	0.002	0.349	186.8	0.66	0.95
Ru/SiO_2-spheres[c]	0.012	0.004	0.006	723.2	0.64	0.95

[a] mass of sample used = 0.1146 g
[b] mass of sample used = 0.0659 g
[c] mass of sample used = 0.2506 g

S3. CO chemisorption on supported RuNPs (raw data).

Table S3a Raw data for CO chemisorption on Ru/SiO_2.

No.	Pe/kPa	P0/kPa	Vd/mL	V/mL(STP) g-1
1	1.58E-01	101.3	18.118	4.31E+00
2	2.08E+00	101.3	18.118	4.95E+00
3	4.549	101.3	18.118	5.02E+00
4	8.7074	101.3	18.118	5.12E+00
5	11.085	101.3	18.118	5.21E+00
6	22.54	101.3	18.118	5.37E+00
7	32.884	101.3	18.118	5.53E+00

Table S3b. Raw data for CO chemisorption on Ru/SBA-15.

No.	Pe/kPa	P0/kPa	Vd/mL	V/mL(STP) g-1
1	6.61E-03	101.3	11.928	7.28E+00
2	2.12E-02	101.3	11.928	1.45E+01
3	1.14E-01	101.3	11.928	2.13E+01
4	2.1634	101.3	11.928	2.88E+01
5	4.7959	101.3	11.928	2.92E+01
6	8.8563	101.3	11.928	2.97E+01
7	10.976	101.3	11.928	30.046
8	24.291	101.3	11.928	30.856
9	33.599	101.3	11.928	31.848

Table S3c. Raw data for CO chemisorption on Ru/SiO_2-spheres.

No.	Pe/kPa	P0/kPa	Vd/mL	V/mL(STP) g-1
1	2.31E+00	101.3	11.016	5.09E-01
2	4.99E+00	101.3	11.016	5.09E-01
3	9.0656	101.3	11.016	5.25E-01
4	11.112	101.3	11.016	5.34E-01
5	24.918	101.3	11.016	5.65E-01
6	34.127	101.3	11.016	5.79E-01

S4. Parameters of the Langmuir fit for supported RuNPs (CO chemisorption).

The CO chemisorption data was fitted with dual non-dissociative Langmuir model (eq. 2):

$$Q_{max} = Q_{ads,1}\frac{K_1P}{1+K_1P} + Q_{ads,2}\frac{K_2P}{1+K_2P} \qquad \text{(eq. 2)}$$

where Q_{max} corresponds to the amount of H_2 adsorbed at saturation, Q_{ads} stands for the quantity of H_2 adsorbed at pressure P, and K represents the equilibrium constant.

Table S4. Parameters of the dual non-dissociative Langmuir for suppored RuNPs (CO – chemisorption).

Sample	**$Q_{ads,1}$ [mole$_{CO}$/g$_{cat}$]**	**K_1**	**$Q_{ads,2}$ [mole$_{CO}$/g$_{cat}$]**	**K_2**	**Q_{max} [mole$_{CO}$/mole$_{Ru}$]**	**R^2**
Ru/SiO_2[a]	0.059	0.022	0.220	43.4	0.94	0.99
Ru/SBA-15[b]	0.351	0.96	1.035	72.2	0.96	0.99
Ru/SiO_2-spheres[c]	0.011	0.011	0.023	15.1	1.1	0.93

[a]mass of sample used = 0.1146 g
[b]mass of sample used = 0.0659 g
[c]mass of sample used = 0.2506 g

S5. Calculation of the mean particle size based on chemisorption results.

For the determination of the particle size of supported RuNPs based on the H_2 and CO chemisorption results, the *hcp* particle model was applied. First, for the *hcp* particle with a shell number of N, the total amount of atoms in the particle (N_{total}) and surface atoms (N_{surf}) were calculated based on the equations taken from Hardeveld et al. *Suf. Sci.* **1969**, *15*, 89-230:

$$N_{total} = \frac{10N^3 + 15N^2 + 11N + 3}{3}$$

$$N_{surf} = 10N^2 + 2$$

Secondly, for the *hcp* particle with a shell number of N, the dispersion (N_{surf}/N_{total}) was calculated. The diameter (D) of the *hcp* particle with the shell number of N was obtained using the equation taken from Blakemore, J. S. *Solid State Physics*, **1985**, Cambridge University Press, Cambridge.

$$D = 2 \times R_{WS} \times N^{1/3}$$

where R_{WS} stands for the Wigner-Seitz radius of a nanoparticle. For Ru the R_{WS} equals 0.147 nm.

Assuming the *hcp* model of a nanoparticle, the relation between a particle size and dispersion was obtained.

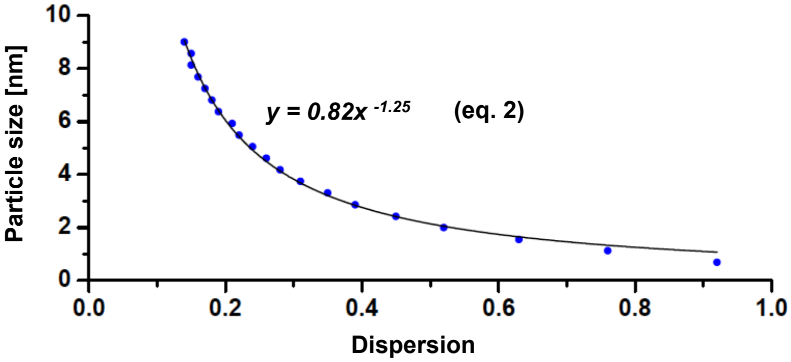

Figure S5. Particle size vs Dispersion relation for *hcp* nanoparticle.

Using the numbers of moles of surface Ru obtained from the chemisorption measurement and by taking into account the number of total moles of Ru used for the measurement, the dispersion of supported RuNPs was calculated. Using the equation obtained from fitting the particle size vs dispersion relation:

$$y = 0.82x^{-1.25}$$

the particle size of supported RuNPs was obtained. The stoichiometry factors used for the particle size estimation were kept constant for both H_2 and CO (2H/$Ru_{surface}$ and 1.5CO/$Ru_{surface}$).

Table S5. Number of atoms (total, surface), dispersion and particle size for the *hcp* particle.

Shell number	**N_{total}**	**$N_{surface}$**	**Dispersion**	**Particle size**
1	13	12	0.92	0.69
2	55	42	0.76	1.12
3	147	92	0.63	1.55
4	309	162	0.52	1.99
5	561	252	0.45	2.42
6	923	362	0.39	2.86
7	1415	492	0.35	3.30
8	2057	642	0.31	3.74
9	2869	812	0.28	4.18
10	3871	1002	0.26	4.62
11	5083	1212	0.24	5.05
12	6525	1442	0.22	5.49
13	8217	1692	0.21	5.93
14	10179	1962	0.19	6.37
15	12431	2252	0.18	6.81
16	14993	2562	0.17	7.25
17	17885	2892	0.16	7.69
18	21127	3242	0.15	8.13
19	24739	3612	0.15	8.57
20	28741	4002	0.14	9.01

S6. Adsorption of CO on RuNPs studied by FTIR.

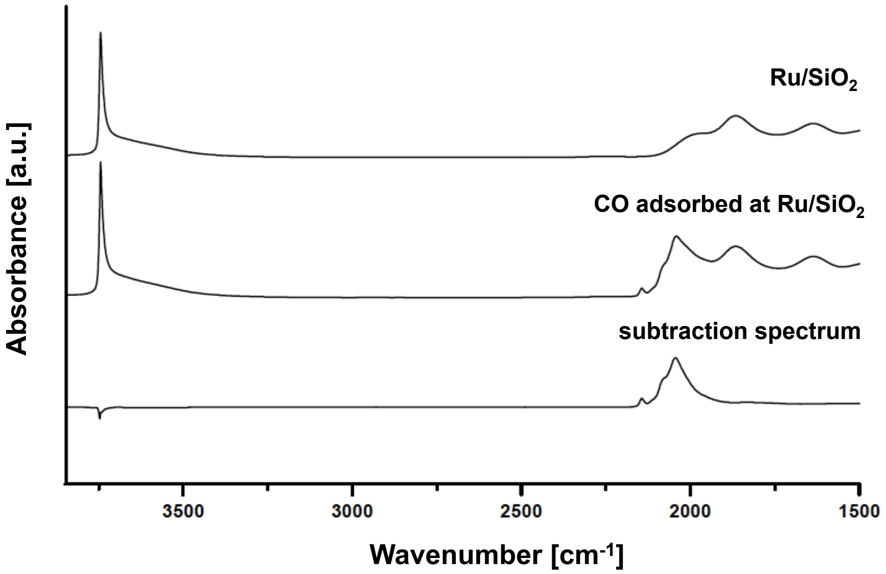

Figure S6. IR spectra of supported RuNPs with and without CO.

S7. Adsorption of ^{13}CO on Ru/SiO_2 (3% wt. Ru). Solid-state ^{13}C NMR study.

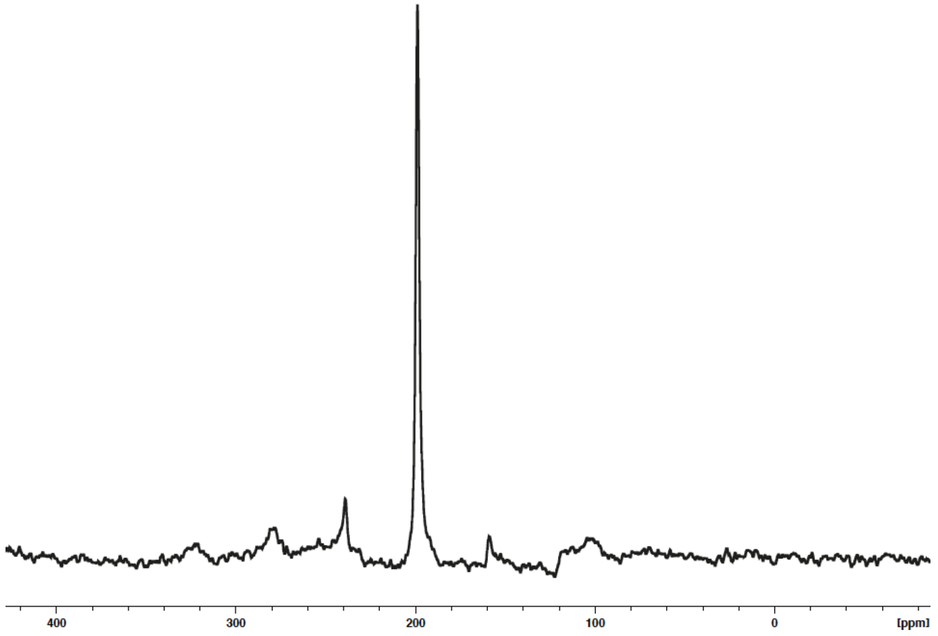

Figure S7. HP-DEC MAS ^{13}C NMR spectrum of ^{13}CO adsorbed on Ru/SiO_2 (3% wt. Ru).

S8. Computational evaluation of the stability of different Ru nanoparticle shapes

Several Ru nanoparticles (NP) containing between 38 and 85 Ru atoms with different particle shapes were constructed. The evaluated geometries correspond to: truncated octahedron (38 atoms), decahedron (54 atoms), icosahedron (55 atoms), ino-decahedron (55 and 85 atoms), cuboctahedron (55 atoms), hcp-based cluster (57 atoms) and Marks truncated decahedron (75 atoms).[10] Their related optimized geometries are depicted in **Figure S8**.

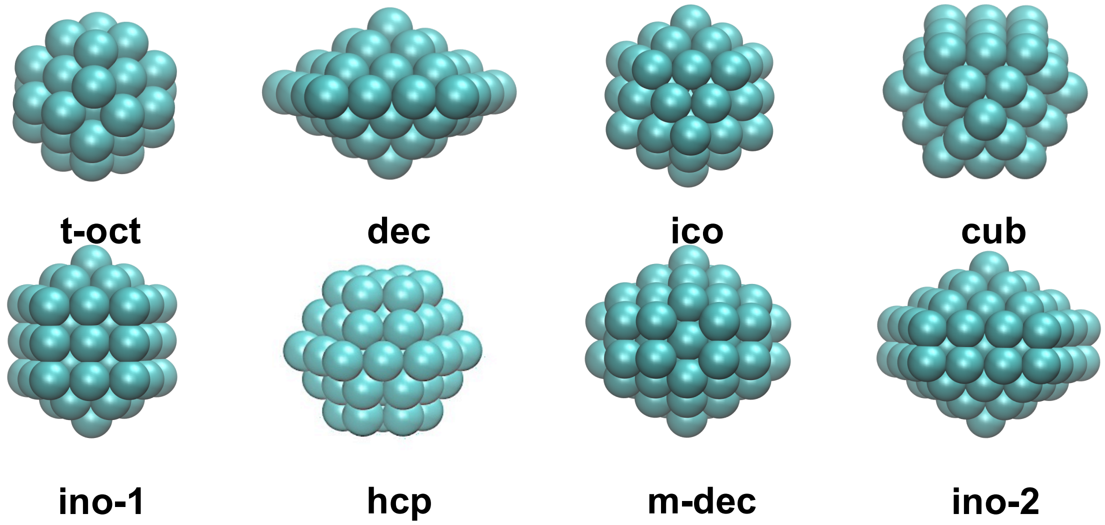

Figure S8. Optimized geometries for all the evaluated Ru nanoparticles.

The cohesive energy per Ru atom in each of the nanoparticles was computed with respect to the energy of a free Ru atom. These results are summarized in Table S6. For the bulk Ru structure a cohesive energy equal to -644 kJ/mol was computed in good agreement with the experimental value (-650 kJ/mol),[11] showing that the PBE functional reproduces with good accuracy the cohesive energy of Ru bulk.

Table S8. Number of Ru atoms and cohesive energy per Ru atom of the different evaluated particle shapes (in kJ.mol^{-1}).

Nanoparticle	Number of atoms	Cohesive energy per Ru atom (kJ.mol^{-1})
t-oct	38	-482
dec	54	-494
ico	55	-497
cub	55	-494
ino-1	55	-498
hcp	57	-503
m-dec	75	-516
ino-2	85	-520

As expected, when increasing the number of Ru atoms in the nanoparticle, the cohesive energy per Ru atom increases. From the data being shown in Table S1 we can already compare the stability of those metal nanoparticles containing the same number of Ru atoms. (icosahedron, cuboctahedron and ino-decahedron). We can see that the ino-decahedron is the most stable structure followed by the icosahedron and the cuboctahedron. In order to compare the energy of nanoparticles containing a different number of metallic atoms, one approximate approach is to plot the difference of cohesive energy of the particles with respect to the bulk (D) as a function of $N^{1/3}$ (**Figure S8**), where N is the number of Ru atoms that contains the nanoparticle. This approach has some limitations and it suggest only trends since it depends on the number of evaluated structures and the slope is sensitive to the inclusion of more data points.

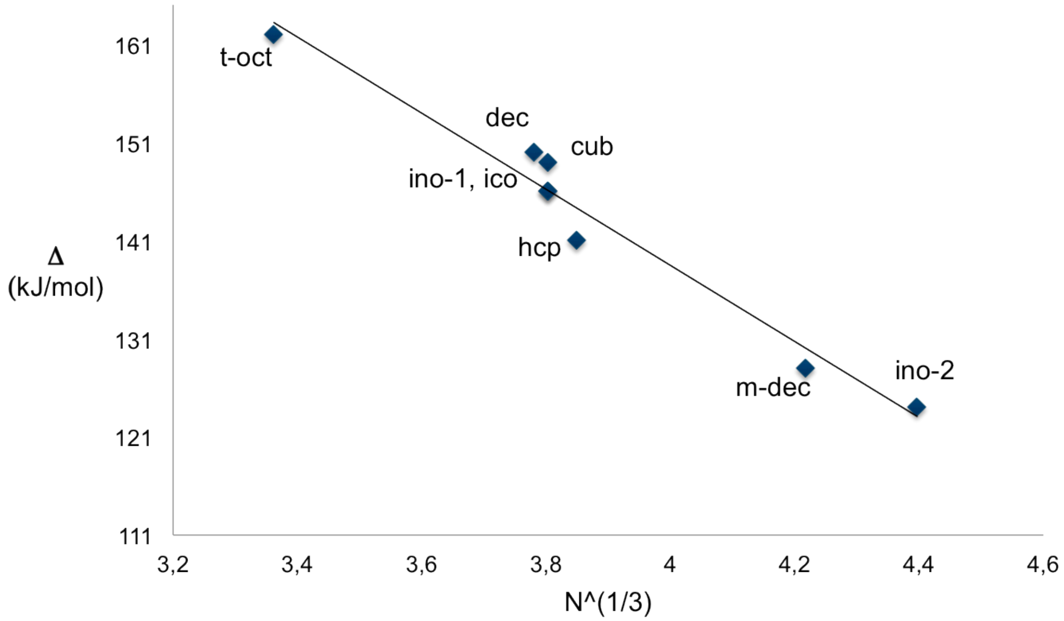

Figure S8. Difference of cohesive energy per Ru atom with respect to the bulk (D, in kJ/mol) as a function of $N^{1/3}$, where N is the number of Ru atoms in the corresponding nanoparticle.

From **Figure S8**, we can observe that the two structures being most deviated to lower Δ values from the regression line are the hcp cluster (with 57 atoms) and the marks-truncated decahedron with 75 atoms. Hence, based on *ab initio* simulations these two structures are the most stable particle shapes for Ru nanoparticles from 38 and to 85 Ru atoms. This is in agreement with the observed particle-shape observed experimentally by HR-TEM images. Hence, based on the agreement between the observed particle shape experimentally and the predicted particle shape based on *ab initio* calculations, in the computational study about the CO and H_2 chemisorption we took the model *hcp* particle, which is composed by 001 and 101 planes and 010 planes.

S9. Summary of the stability of structures containing the same CO coverage (for 0.5 CO, 1.0 CO and 1.5 CO ML).

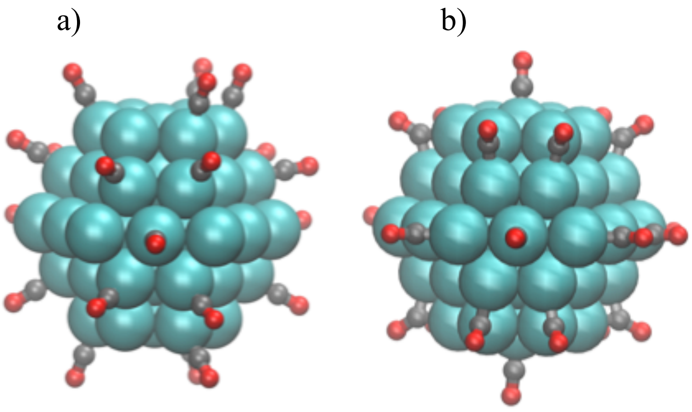

$E_{bind/CO}$ = -179 kJ/mol $E_{bind/CO}$ = -187 kJ/mol

Figure S9.1 Two evaluated configurations for the 0.5 ML CO coverage. a) CO adsorbed on the T6, T3 and half of the T2 sites. b) CO adsorbed on B3, T1 and all the B8 sites except one. The binding energy per CO molecule is given for both structures.

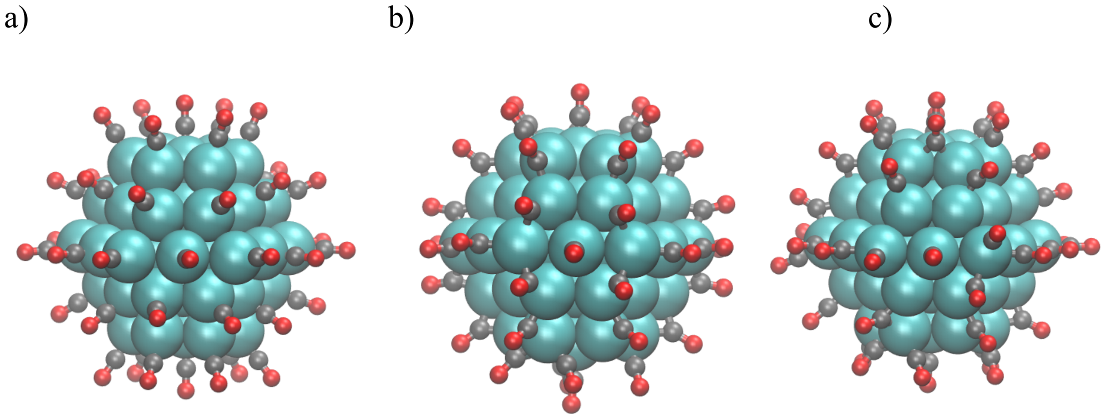

$E_{bind/CO}$ = -165 kJ/mol $E_{bind/CO}$ = -173 kJ/mol $E_{bind/CO}$ = -174 kJ/mol

Figure S9.2. Three evaluated configurations for 1 CO ML adsorbed on the hcp nanoparticle. a) Adsorption on all the top sites. b) Adsorption on the T6, T1, B8, B2, B7 and three B1 sites. c) Adsorption on the T6, T1, B8, T5 and a mix of B3, B1, T2, T3 and B7 sites. The binding energy per CO molecule is given for the three structures.

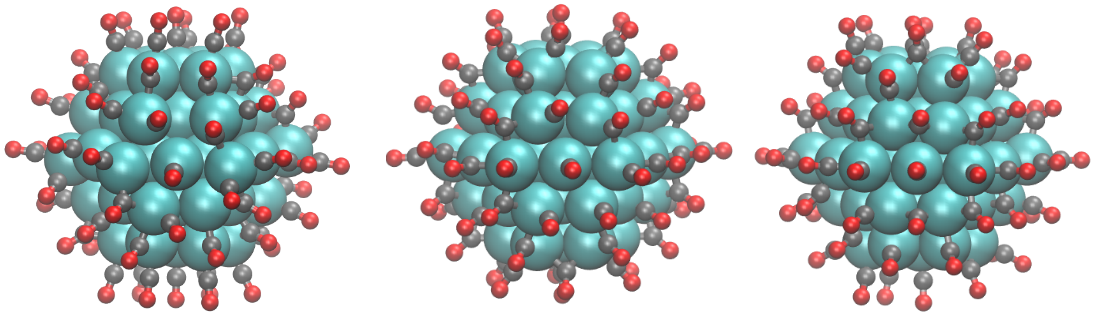

$E_{bind/CO}$ = -147 kJ/mol $E_{bind/CO}$ = -151 kJ/mol $E_{bind/CO}$ = -150 kJ/mol

Figure S9.3 Three evaluated configurations for 1.5 CO ML adsorbed on the hcp nanoparticle. a) Adsorption on all the top sites were the CO molecules were initially placed on all the B3 and some H3 sites. b) Structure constructed from the most stable structure for a 1 CO ML coverage. c) Similar to the b) where the position of the CO molecules is slightly different. The binding energy per CO molecule is given for the three structures.

S10. Stability of the CO and H coverages as a function of ΔμCO and ΔμH.

The expected coverage for a given value of $\Delta\mu_{CO}$ will be the one that has a more favorable reaction energy (more negative ΔG). We will divide the complete surface phase diagram in different graphs. The first diagram shows the phase of diagram CO coverages between 0 and 0.93 CO ML (**Figure S10.1**). We see how at $\Delta\mu_{CO}$ around -2 eV, the 0.38 CO ML coverage becomes more stable than the clean nanoparticle. Then, for a small range of $\Delta\mu_{CO}$ from 1.8 eV, the 0.5 CO ML becomes the most stable phase. Afterwards, there is a range in which 0.66 ML becomes the most stable coverage, until around -1.65 eV, where the 0.93 CO ML is the most stable one. The 0.79 CO ML is not found as most stable phase.

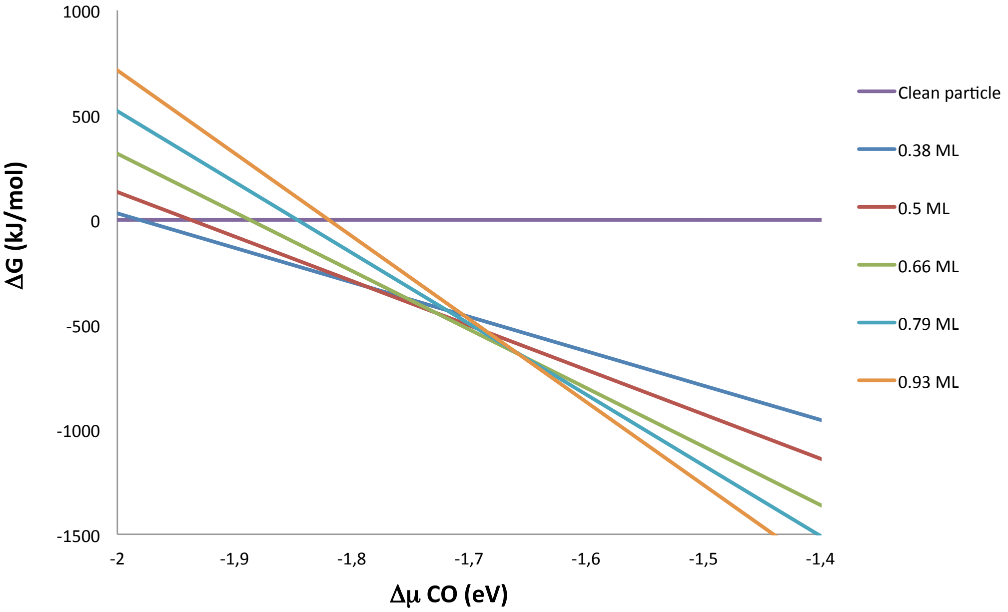

Figure S10.1. Total adsorption energy (ΔG, in kJ.mol^{-1}) of CO on the hcp-based nanoparticle for coverages between 0.38 and 0.93 CO ML.

Next, we will describe the CO coverages between 0.93 and 1.34 CO ML. From **Figure S10.2**, we can observe how at $\Delta\mu_{CO}$ equal to -1.6 eV, the 1 CO ML coverage becomes more stable than the 0.93 CO ML, which was the most stable coverage from -1.65 eV. The next stable coverage is 1.15 ML, which crosses the line of 1 CO ML around -1.35 eV. This coverage is the most stable one until a $\Delta\mu_{CO}$ of -1.1 eV, where the 1.34 CO ML coverage becomes the most stable one.

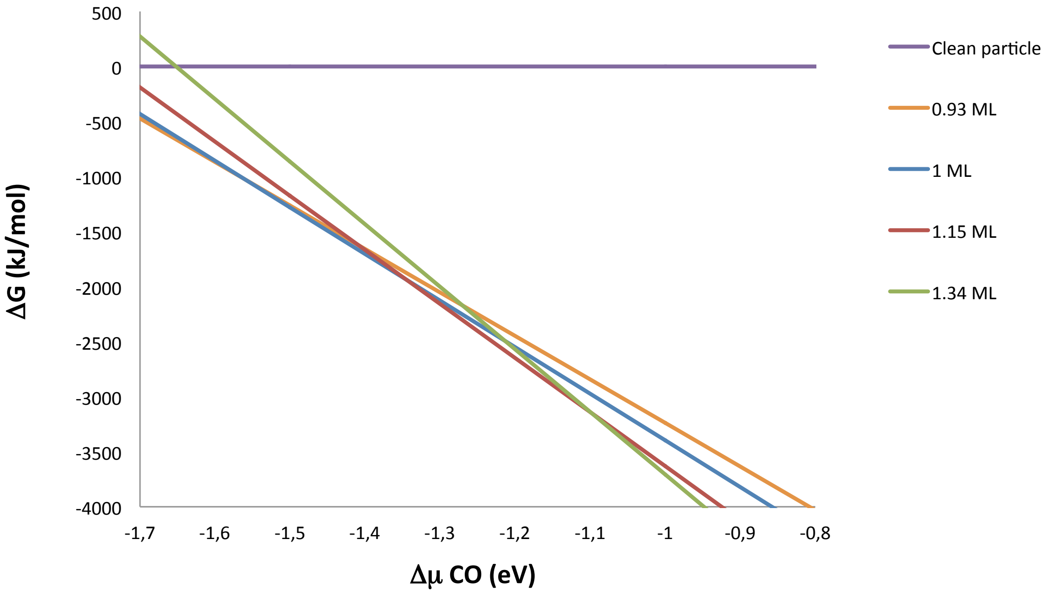

Figure S10.2. Total adsorption energy (ΔG, in kJ.mol^{-1}) of CO on the hcp-based nanoparticle for coverages between 0.93 and 1.34 CO ML.

At **Figure S10.3**, they are represented the most stable CO coverages between 1.34 and 1.61 CO ML.

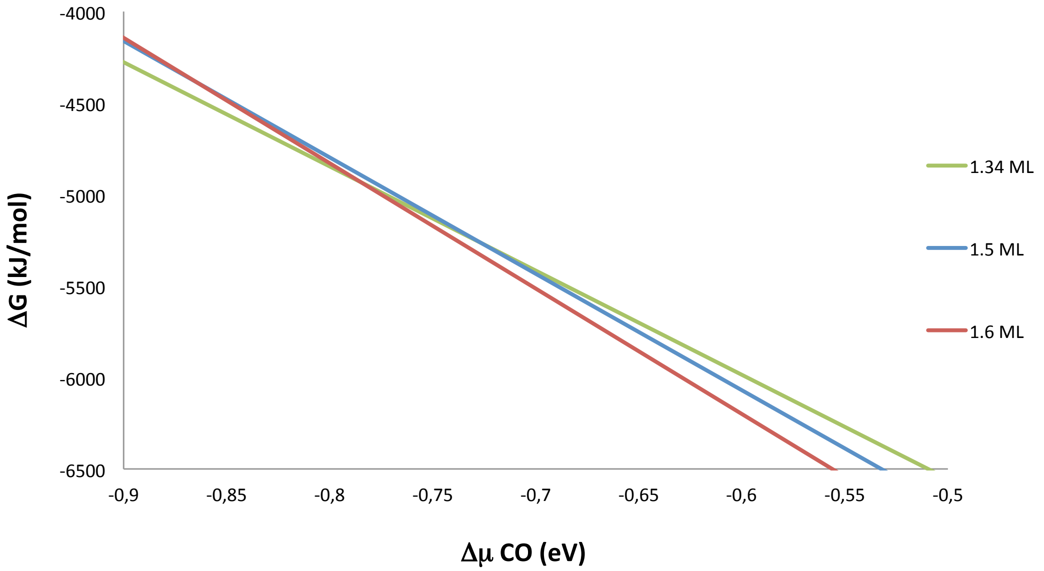

Figure S10.3. Total adsorption energy (ΔG, in kJ.mol^{-1}) of CO on the hcp-based nanoparticle for coverages between 1.34 and 1.6 CO ML as function of the variation of the CO chemical potential ($\Delta\mu_{CO}$ in eV).

We can see how 1.34 CO ML is stable until around -0.8 eV and the next most stable phase is 1.61 CO ML around -0.78 eV. This phase is actually stable for significant range of $\Delta\mu_{CO,}$ until 1.66 ML becomes the most stable phase until around -0.26 eV The next phase, which is stable under a given chemical potential is the 1.86 CO ML (**Figure S10.4**) Note than none of the intermediate coverages. e. g. 1.71, 1.75 and 1.81 CO ML is the most stable phase at any value of $\Delta\mu_{CO.}$

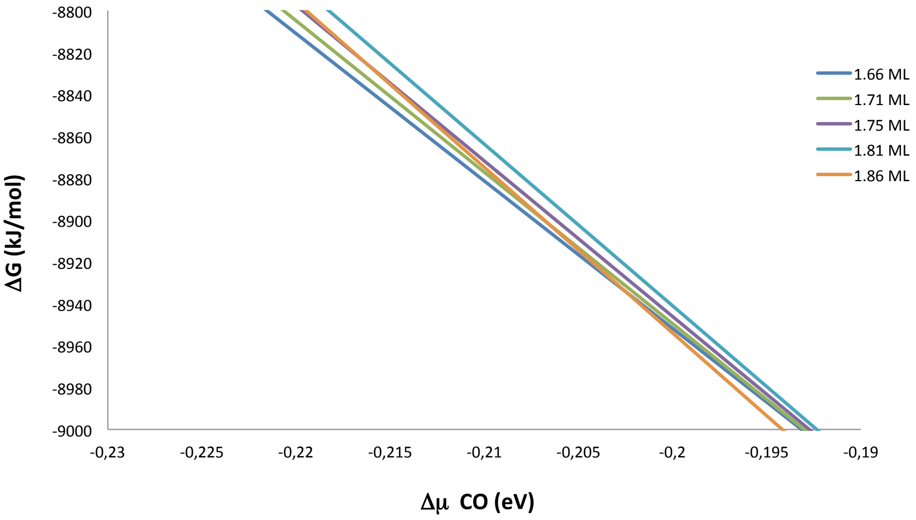

Figure S10.4. Total adsorption energy (ΔG, in kJ.mol^{-1}) of CO on the hcp-based nanoparticle for the CO coverages between 1.66 and 1.86 CO ML as function of the variation of the CO chemical potential ($\Delta\mu_{CO}$ in eV).

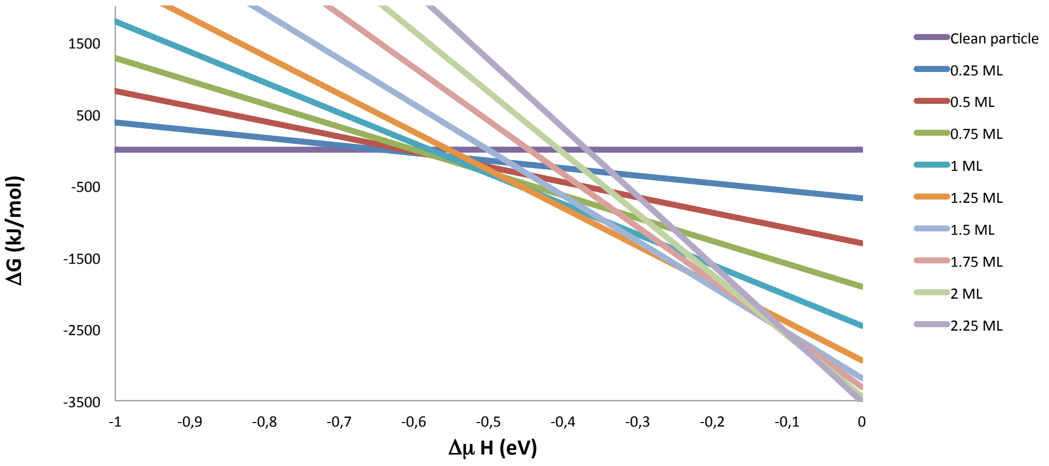

Figure S10.5. Total adsorption energy (ΔG, in $kJ.mol^{-1}$) of atomic H on the hcp-based nanoparticle for different H coverages as function of the variation of the H chemical potential (in eV).

References

1. Berthoud, R.; Délichère, P.; Gajan, D.; Lukens, W.; Pelzer, K.; Basset, J.-M.; Candy, J.-P.; Copéret, C., *J. Catal.* **2008,** *260*, 387-391.
2. Furman, K.; Baudouin, D.; Margossian, T.; Sabnis, K. D.; Cui, Y.; Ribeiro, F. H.; Copéret, C., *J. Catal.* **2015,** *324*, 9-13.
3. Low, J. E.; Foelske-Schmitz, A.; Krumeich, F.; Worle, M.; Baudouin, D.; Rascon, F.; Coperet, C., *Dalton Trans.* **2013,** *42*, 12620-12625.
4. (a) Kresse, G.; Furthmüller, J., *Comput. Mat. Sci.* **1996,** *6*, 15; (b) Kresse, G.; Furthmüller, J., *Phys. Rev. B* **1996,** *54*, 11169.
5. (a) Perdew, J. P.; Burke, K.; Ernzerhof, M., *Phys. Rev. Lett.* **1996,** *77*, 3865; (b) Perdew, J. P.; Burke, K.; Ernzerhof, M., *Phys. Rev. Lett.* **1997,** *78*, 1396.
6. (a) Blöchl, P. E., *Phys. Rev. B* **1994,** *50*, 17953; (b) Kresse, G.; Joubert, D., *Phys. Rev. B* **1999,** *59*, 1758.
7. Zhang, Y.; Yang, W., *Phys. Rev. Lett.* **1998,** *80*, 890-890.
8. Reuter, K.; Scheffler, M., *Phys. Rev. B* **2001,** *65*, 035406.
9. Stull, D. R.; Prophet, H., JANAF Thermochemical Tables, 2nd edn. U.S. National Bureau of Standards (U.S. EPO): Washington D. C., 1971.
10. Marks, L. D., *Philosophical Magazine A* **1984,** *49*, 81-93.
11. Kittel, C., *Introduction to Solid-State Physics*. Wiley: New York, 2005.